

Spiral Instabilities in Rayleigh-Bénard Convection under Localized Heating

M. C. Navarro¹, A. M. Mancho² and H. Herrero¹

¹ Departamento de Matemáticas Facultad de Ciencias Químicas
Universidad de Castilla-La Mancha 13071 Ciudad Real, Spain.

² Instituto de Matemáticas y Física Fundamental
Consejo Superior de Investigaciones Científicas
Serrano 121, 28006 Madrid, Spain.

Abstract

We study from the numerical point of view, instabilities developed in a fluid layer with a free surface, in a cylindrical container which is non-homogeneously heated from below. In particular we consider the case in which the applied heat is localized around the origin. An axysymmetric basic state appears as soon a non-zero horizontal temperature gradient is imposed. The basic state may bifurcate to different solutions depending on vertical and lateral temperature gradients and on the shape of the heating function. We find different kinds of instabilities: extended patterns growing on the whole domain which include those known as targets and spirals waves. Spirals are present even for infinite Prandtl number. Localized structures both at the origin and at the outer part of the cylinder may appear either as Hopf or stationary bifurcations. An overview of the developed instabilities as a function of the dimensionless parameters is reported in this article.

Corresponding author: Ana M. Mancho, Instituto de Matemáticas y Física Fundamental, Consejo Superior de Investigaciones Científicas, Serrano 121, 28006, Madrid. Phone: +34 91 5616800 ext 2408. Fax: +34 91 5854894. e-mail: A.M.Mancho@mat.csic.es

Spiral and target waves instabilities in Rayleigh-Bénard convection were experimentally found in early nineties and several theoretical mechanisms have been proposed to justify them. In this article we prove that these and other structures may be understood as the linearly growing modes of non trivial basic states generated by a non uniform heating function. In this framework we find that also localized structures may appear. These patterns are localized at different positions in the domain depending on the basic flow from which they bifurcate. This article reports a systematical numerical study on these transitions.

1 Introduction

Instabilities and pattern formation in buoyant flows have been extensively studied in recent years. Classically, heat is applied uniformly from below [1] and the conductive solution (also called the basic solution) becomes unstable for a critical vertical temperature gradient beyond a certain threshold. Typically, instabilities in Rayleigh-Bénard convection lead to roll patterns, however spiral waves have been also reported, in both theoretical and experimental results. First experimental observations on spirals [2, 3] in Rayleigh-Bénard convection were rather surprising as they were carried out for a set of external parameter values where parallel rolls should be stable. In experiments, spirals have been reported for finite Prandtl number [4] and both single and multiarmed giant spirals and spiral chaos have been observed. In [5] transitions between spiral and target states are reported. First theoretical studies attempting to justify spiral patterns in Rayleigh Bénard convection were performed just in model equations such as Swift-Hohenberg type equations [6, 7]. These results were confirmed by later simulations of the full governing equations [8, 9].

A more general setup for Rayleigh-Bénard convection than the case of uniform heating, consists of a basic dynamic flow imposed by a non-zero horizontal temperature gradient which may be either constant or not. Numerical results obtained at the former setup in an annular domain address the importance of both vertical and horizontal temperature gradients in the development of instabilities [18, 20, 21, 22]. In this work we consider a cylindrical domain with a localised Gaussian-like heating at the bottom. Therefore, apart from vertical and horizontal temperature gradients, a heat parameter related to the shape of the heating profile at the bottom is introduced. Our results show that many different types of instabilities may appear depending on the basic flow and external parameters. We study how instabilities depend on dimensionless parameters and we recover many results as those described for the classical uniform heating case. Giant single armed spiral waves appear and their instability threshold is close to those patterns referred as targets. Localised and extended spirals are identified and both of them are found for finite and infinite Prandtl number. Moreover, stationary patterns appear both with local and extended structure.

The paper is organized as follows. Section 2 describes the physical setup, the general mathematical formulation of the problem in a dimensionless form, for basic solutions and their linear stability analysis. Section 3 explains the numerical method in detail and presents a test of convergence. In section 4 the numerical results on both, the basic and growing perturbations, are discussed and conclusions are presented.

2 Formulation of the problem

The physical set up (see figure 1) consists of a horizontal fluid layer in a cylindrical container of radius l (r coordinate) and depth d (z coordinate). The upper surface is open to the atmosphere and the bottom plate is rigid. At $z = 0$ the

imposed temperature is a Gaussian profile which takes the value T_{\max} at $r = 0$ and the value T_{\min} at the outer part ($r = l$). The environmental temperature is T_0 . We define $\Delta T_v = T_{\max} - T_0$, $\Delta T_h = T_{\max} - T_{\min}$ and $\delta = \Delta T_h / \Delta T_v$.

In the equations governing the system u_r , u_ϕ and u_z are the components of the velocity field u , T is the temperature, p is the pressure, r is the radial coordinate and t is the time. The magnitudes are expressed in dimensionless form after rescaling in the following form: $\mathbf{r}' = \mathbf{r}/d$, $t' = \kappa t/d^2$, $u' = du/\kappa$, $p' = d^2 p / (\rho_0 \kappa \nu)$, $\Theta = (T - T_0) / \Delta T$. Here \mathbf{r} is the position vector, κ the thermal diffusivity, ν the kinematic viscosity of the liquid and ρ_0 is the mean density at the environment temperature T_0 . After rescaling the domain $\Omega_1 = [0, l] \times [0, d]$ is transformed into $\Omega_2 = [0, \Gamma] \times [0, 1]$ where $\Gamma = l/d$ is the aspect ratio

The system evolves according to the momentum and the mass balance equations and to the energy conservation principle, which in dimensionless form are (the primes in the corresponding fields have been dropped),

$$\nabla \cdot u = 0, \quad (1)$$

$$\partial_t \Theta + u \cdot \nabla \Theta = \nabla^2 \Theta, \quad (2)$$

$$\partial_t u + (u \cdot \nabla) u = \text{Pr} (-\nabla p + \nabla^2 u + \text{R} \Theta e_z), \quad (3)$$

where the operators and fields are expressed in cylindrical coordinates and the Oberbeck-Boussinesq approximation has been used. Here e_z is the unit vector in the z direction. The following dimensionless numbers have been introduced: the Prandtl number $\text{Pr} = \nu/\kappa$ and the Rayleigh number $\text{R} = g\alpha\Delta T d^3/\kappa\nu$, which represents the buoyant effect. In these definitions α is the thermal expansion coefficient and g is the gravity constant.

We discuss now the boundary conditions (bc). The top surface is flat, which implies the following condition on the velocity,

$$u_z = 0, \quad \text{on } z = 1. \quad (4)$$

and free slip,

$$\partial_z u_r = 0, \quad \partial_z u_\phi = 0, \quad \text{on } z = 1. \quad (5)$$

Lateral and bottom walls are rigid, so

$$u_r = u_\phi = u_z = 0, \quad \text{on } z = 0, \quad (6)$$

$$u_r = u_\phi = u_z = 0, \quad \text{on } r = \Gamma. \quad (7)$$

For temperature we consider the dimensionless form of Newton's law for heat exchange at the surface,

$$\partial_z \Theta = -B\Theta, \quad \text{on } z = 1, \quad (8)$$

where B is the Biot number. At the bottom a gaussian profile is imposed,

$$\Theta = 1 - \delta (e^{(\frac{1}{\beta})^2} - e^{(\frac{1}{\beta} - (\frac{\#}{\beta})^2 \frac{1}{\beta})^2}) / (e^{(\frac{1}{\beta})^2} - 1) \quad \text{on } z = 0, \quad (9)$$

where β is a measure of the sharpness of the profile. In figure 2 several plots of this profile for different values of the parameters can be seen. The lateral wall is insulating,

$$\partial_r \Theta = 0 \quad \text{on} \quad r = \Gamma. \quad (10)$$

The use of cylindrical coordinates, which are singular at $r = 0$, requires regularity conditions on velocity, pressure and temperature fields. In general, these conditions are expressed as follows [30]

$$\frac{\partial(u_r e_r + u_\phi e_\phi)}{\partial \phi} = \partial_\phi u_z = \partial_\phi p = \partial_\phi \Theta = 0 \quad \text{on} \quad r = 0, \quad (11)$$

where e_r and e_ϕ are the unit vectors in the r and ϕ directions respectively. To summarize, the dimensionless equations contains these external parameters ($R, \Gamma, Pr, \delta, B, \beta$). Our aim is to describe the type of bifurcations that appear when some of those dimensionless quantities are varied.

2.1 Basic state and linear stability analysis

The horizontal temperature gradient at the bottom (i.e. $\delta \neq 0$) settles a stationary convective motion which is called basic state. It is a time independent solution to the stationary problem obtained from equations (1-3). The basic state is axisymmetric therefore it depends only on $r - z$ coordinates (i.e. all ϕ derivatives are zero). The velocity field of the basic flow is restricted to $u = (u_r, u_\phi = 0, u_z)$. Regularity conditions (11) now become

$$u_r = \partial_r u_z = \partial_r p = \partial_r \Theta = 0 \quad \text{on} \quad r = 0. \quad (12)$$

We have solved numerically the simplified equations for the basic state together with its boundary conditions. We use a Chebyshev collocation method with details given in section 3.

The stability of the basic state is studied by perturbing it with a vector field depending on the r, ϕ and z coordinates, in a fully 3D analysis:

$$u_r(r, \phi, z) = u_r^b(r, z) + \bar{u}_r(r, z) \exp(ik\phi + \lambda t), \quad (13)$$

$$u_\phi(r, \phi, z) = u_\phi^b(r, z) + \bar{u}_\phi(r, z) \exp(ik\phi + \lambda t), \quad (14)$$

$$u_z(r, \phi, z) = u_z^b(r, z) + \bar{u}_z(r, z) \exp(ik\phi + \lambda t), \quad (15)$$

$$\Theta(r, \phi, z) = \Theta^b(r, z) + \bar{\Theta}(r, z) \exp(ik\phi + \lambda t), \quad (16)$$

$$p(r, \phi, z) = p^b(r, z) + \bar{p}(r, z) \exp(ik\phi + \lambda t). \quad (17)$$

Here the superscript b indicates the corresponding quantity in the basic state and the bar refers to the perturbation. We have considered Fourier mode expansions in the angular direction, because along it boundary conditions are periodic. Expressions (13-17) are replaced into basic equations (1-3) and the resulting system is linearized. Boundary conditions for perturbations ($\bar{u}_r, \bar{u}_\phi, \bar{u}_z, \bar{\Theta}, \bar{p}$)

are found by substituting (13-17) into (4-11). Regularity conditions (11) depend now on the wavenumber k :

$$\bar{u}_r = \bar{u}_\phi = \frac{\partial \bar{u}_z}{\partial r} = \frac{\partial \bar{\Theta}}{\partial r} = \frac{\partial \bar{p}}{\partial r} = 0, \text{ for } k = 0, \quad (18)$$

$$\bar{u}_r + i\bar{u}_\phi = \bar{u}_z = \bar{\Theta} = \bar{p} = 0, \text{ for } k = 1, \quad (19)$$

$$\bar{u}_r = \bar{u}_\phi = \bar{u}_z = \bar{\Theta} = \bar{p} = 0, \text{ for } k \neq 0, 1. \quad (20)$$

The resulting problem is an eigenvalue problem in λ . If $Re(\lambda) < 0$ for all eigenvalues the basic state is stable while if there exists a value of λ such as $Re(\lambda) > 0$ the basic state becomes unstable. The condition $Re(\lambda) = 0$ may be satisfied for certain values of the external parameters, $(R, \Gamma, Pr, \delta, B, \beta)$, which define the critical threshold. At the critical threshold, a stationary bifurcation takes place if $Im(\lambda) = 0$ while it is a Hopf bifurcation if $Im(\lambda) \neq 0$.

3 Numerical method

We have solved both the basic state and the linear stability problem as stated in (1-3), i.e. in primitive variables formulation by expanding the fields with Chebyshev polynomials (see Ref. [28]). Using this technique, the problem of the spurious modes for pressure arises [28, 29], which we have solved using the method proposed in [30], taking additional boundary conditions. They are obtained by the continuity equation at $z = 0$ and the normal component of the momentum equations on $r = \Gamma$ and $z = 1$,

$$\nabla \cdot u = 0, \text{ on } z = 0, \quad (21)$$

$$\begin{aligned} & Pr^{-1} \left(\frac{\partial u_r}{\partial t} + u_r \frac{\partial u_r}{\partial r} + \frac{u_\phi}{r} \frac{\partial u_r}{\partial \phi} + u_z \frac{\partial u_r}{\partial z} - \frac{u_\phi^2}{r} \right) = \\ & = -\frac{\partial p}{\partial r} + \Delta u_r - \frac{u_r}{r^2} - \frac{2}{r^2} \frac{\partial u_\phi}{\partial \phi}, \text{ on } r = \Gamma, \end{aligned} \quad (22)$$

$$\begin{aligned} & Pr^{-1} \left(\frac{\partial u_z}{\partial t} + u_r \frac{\partial u_z}{\partial r} + \frac{u_\phi}{r} \frac{\partial u_z}{\partial \phi} + u_z \frac{\partial u_z}{\partial z} \right) = \\ & = -\frac{\partial p}{\partial z} + \Delta u_z + R\Theta, \text{ on } z = 1, \end{aligned} \quad (23)$$

where $\Delta = r^{-1} \partial / \partial r (r \partial / \partial r) + r^{-2} \partial^2 / \partial \phi^2 + \partial^2 / \partial z^2$.

3.1 Basic state

We have solved numerically the stationary axisymmetric version of equations (1-3) together with the boundary conditions, by treating the nonlinearity with a Newton-like iterative method. In a first step the nonlinearity was neglected and a solution was found by solving the linear system: $u_r^0, u_\phi^0, u_z^0, p^0, \Theta^0$. This solution was corrected by perturbation fields: $u_r^1 = u_r^0 + \bar{u}_r$, $u_z^1 = u_z^0 + \bar{u}_z$, $p^1 = p^0 + \bar{p}$ and $\Theta^1 = \Theta^0 + \bar{\Theta}$. These expressions are introduced into the

equations which are linearized around the approach at step 0. This procedure is repeated with the new solution and so on. The criterion of convergence considered to stop the iterative procedure is that the l^2 norm of the computed perturbation should be less than 10^{-9} .

At each step the resulting linear system for perturbations is solved by expanding any unknown perturbation field \mathbf{x} in Chebyshev polynomials,

$$\mathbf{x} = \sum_{l=0}^{L-1} \sum_{n=0}^{N-1} a_{ln}^{\mathbf{x}} T_l(r) T_n(z). \quad (24)$$

For computational convenience the domain $\Omega_2 = [0, \Gamma] \times [0, 1]$ is transformed into $\Omega = [-1, 1] \times [-1, 1]$. This change of coordinates introduces scaling factors in equations and boundary conditions which are not explicitly given here. There are $4 \times L \times N$ unknowns which are determined by a collocation method. In particular, expansions (24) are replaced into the linearized, stationary, axisymmetric equations and boundary conditions, and those are posed at the Gauss-Lobatto collocation points (r_j, z_i) ,

$$r_j = \cos\left(\left(\frac{j-1}{L-1} - 1\right)\pi\right), \quad \forall j = 0 \dots L. \quad (25)$$

$$z_i = \cos\left(\left(\frac{i-1}{N-1} - 1\right)\pi\right), \quad \forall i = 0 \dots N. \quad (26)$$

Evaluation rules are as follows: the conveniently simplified Eqs. (1-3) are evaluated at nodes $i = 2, \dots, N-1$, $j = 2, \dots, L-1$; the boundary conditions at $z = -1$, (6) and (9) at $i = 1$, $j = 2, \dots, L-1$; the boundary conditions at $z = 1$, (4-5) and (8) at $i = N$, $j = 2, \dots, L-1$; the boundaries at $r = -1$, (12) at $i = 1, \dots, N$, $j = 1$; finally the boundaries at $r = 1$, (7) and (10) at $i = 1, \dots, N$, $j = L$. The system of equations is completed with additional boundary conditions that eliminate spurious modes for pressure. At $z = -1$ equation (21) is evaluated at nodes $i = 1$, $j = 2, \dots, L-1$; at $z = 1$ equation (23) is evaluated at nodes $i = N$, $j = 2, \dots, L$; at $r = 1$ equation (22) is evaluated at $i = 1, \dots, N-1$, $j = L$. With these rules the matrix associated to the linear algebraic system is singular, due to the fact that pressure is defined up to an additive constant. To fix this constant the boundary condition (22) in node $i = N-2, j = L$ is replaced by a Dirichlet condition for pressure (*i.e.*, $p = 0$ at $i = N-2, j = L$). In this way at each iteration step a linear system of the form $AX = B$ is obtained, where X is a vector containing $4 \times L \times N$ unknowns and A is full rank matrix of order $P \times P$ with $P = 4 \times L \times N$. This can be easily solved with standard routines.

3.2 Linear stability analysis

The eigenvalue problem described in section 3.1 is discretized by expanding perturbations (13-17) in a truncated series of orthonormal Chebyshev polynomials as we did with the basic state. These expressions are replaced into the linearized

version of equations (1-3) and boundary and regularity conditions (4-11). We use as in the previous subsection a collocation method where equations are evaluated at the Gauss-Lobatto points. Evaluation rules are analogous except that now regularity conditions are replaced by those expressed in (18-20). We notice that for $k = 1$ there are only four boundary conditions at $r = -1$, and therefore in order to fit the unknowns with the equations we have diminished the expansion range of the u_ϕ field by one order,

$$u_\phi = \sum_{l=0}^{L-2} \sum_{n=0}^{N-1} a_{ln}^v T_l(r) T_n(z).$$

In this way for $k = 1$ we have $P = 4 \times N \times L + N \times (L - 1)$ unknowns and equations while these are $P = 5 \times L \times N$ for $k > 1$ and $P = 4 \times L \times N$ for $k = 0$. For the eigenvalue problem these rules are explicitly detailed in Ref. [30] with the sole difference that here equations are linearized around a non trivial basic state instead of around a conductive solution.

The eigenvalue problem is then transformed into its discrete form

$$Aw = \lambda Bw \quad (27)$$

where w is a vector which contains P unknowns and A and B are $P \times P$ matrices. The discrete eigenvalue problem (27) has a finite number of eigenvalues λ_i . The stability condition explained in previous subsection must be required now upon λ_{\max} where $\lambda_{\max} = \max Re(\lambda_i)$. In Ref. [33] many details on how to solve this problem efficiently are given.

As in [20], we have carried out a test on the convergence of the method that let us assure the correctness of the results. Table I shows some results on convergence rates. We find that expansions of order 33×9 are enough to ensure accuracy within 1%.

4 Numerical Results

In this section we describe numerical results found for different values of external parameters. The problem formulated through Eqs. (1-11) depends on the dimensionless numbers ($R, \Gamma, Pr, \delta, B, \beta$). In particular we are interested in analyzing how those parameters related to heat conditions impose basic flows leading to a great variety of instabilities. Some of them such as giant spirals or targets have been already described in experiments for the case of Rayleigh-Bénard convection with uniform heating [2, 4, 5].

Issues related to horizontal and vertical temperature differences have already been addressed in [20, 21, 22] but here we study for the first time the influence of the shape parameter β . We restringe ourselves to large and medium β values, i.e. $\beta > 0.5$. In this region the numerical method has good convergence and among other instabilities a giant spiral is observed. Smaller β values will be addressed in future works. We also analyze the influence of δ measuring the quotient between lateral and vertical temperature gradients. Figure 2a) illustrates the

dependence of the temperature boundary condition on β while figure 2b) shows its dependence on δ .

4.1 Basic states

We have solved numerically the stationary axisymmetric version of equations (1-3) together with the boundary conditions, as explained in section 3.1. Different basic state solutions are obtained depending on the parameters. Figure 3a) displays a return flow with clearly inverted temperature gradients and a single roll on the velocity field. Figure 3b) shows a linear temperature field with no inversions on the temperature gradient and several corotative rolls. Figures 3c) and 3d) displays intermediate states. In Figure 3c) we see a rather vertical temperature gradients with slight inversions and a slight corotative roll. Figure 3d) displays a return flow where the outer part of the cylinder is hotter than the inner one. These basic flows become unstable to different spatial structures as we explain next.

4.2 Instabilities

We have studied numerically the linear stability of the numerical basic states following explanations of section 3.2. We consider the external parameter R as control parameter. By control parameter we mean the parameter that changed leads to an instability while all the others are fixed. This occurs when $\lambda_{\max}(R)$ changes from a negative value to a positive one as R varies. The value of R_c for which $\lambda_{\max}(R_c) = 0$ is the critical value. Figure 4 displays $\lambda_{\max}(R_c)$ as a function of the wave number k and all other parameters fixed. The eigenvalue with maximum real part corresponds to $k = 15$ and as it is purely real, the bifurcation is stationary. Depending on the different parameters a great variety of instabilities are obtained either stationary or oscillatory with different growing modes, which are analyzed next.

4.2.1 Influence of β and δ

In this section we study how the shape factor β and the temperature quotient δ both related to the bottom heat boundary condition affect to the instabilities. To start with we fix parameters $\Gamma = 10$, $\text{Pr} = 0.4$ and $B = 0.05$ and take R as control parameter. Figures 5a and 5b display critical values of R_c as a function of δ for $\beta = 0.5$ and $\beta = 5$, respectively. Critical wave numbers k_c and the corresponding growing modes are shown in these figures where void circles correspond to stationary bifurcations while crossed ones stand for oscillatory instabilities. Both figures show regions with qualitatively different behaviors which are separated by vertical lines. In figure 5a for $\delta > 0.15$ and in figure 5b for $\delta > 0.055$ the critical R increases when δ decreases. At the δ limit values, the R threshold tends to grow so much that we have not found it. This suggests that there is an asymptote where the critical R_c tends to infinity. As δ is increased, the control parameter R decreases and so does the critical wave

number. Comparing figures 5a and 5b, which differ in its β values, we notice more localized bifurcating structures for small values of β . This part of the diagram is called region I. At different β the critical R_c tends to infinity at different δ values. In figure 6, the curve C_1 (solid line) that limits region I marks the position of this asymptote in the $\beta - \delta$ plane. An example of a basic state in region I is presented in Figure 3a). It corresponds to a return flow.

In figure 5b, at $-0.05 < \delta < 0.055$, an oscillatory bifurcation is obtained with wave number $k = 0$. This is detailed in figure 5c, where a zoom of this region is displayed. The critical R_c tends to infinity as δ tends to the interval limits. The oscillatory mode $k = 1$ is just below the instability threshold but very close to it, at the same parameter values. Figure 7 displays the values of $\lambda_{\max}(R_c)$ as a function of the wave number k . The zero mode is the preferred one, but as the mode one is so close to it, it could be possible that both modes appear after the bifurcation. The mode $k = 0$ corresponds to a target pattern (see figure 8a) and the mode $k = 1$ to a giant one-armed spiral (see figure 8b). These plots represent contours of the growing temperature field eigenfunction and their structure are quite similar to those described in [2, 3, 4, 5]. The zone where we find these behaviours is called zone II (see figure 6). We do not find such instabilities for $\beta = 0.5$. In fact they exist only for large enough β values in a small interval around $\delta = 0$, excluding $\delta = 0$. This is clearly depicted in Figure 6 where curve C_2 (dashed- dotted line) limits region II. Figure 3b) displays an example of a basic state in region II. It corresponds to a linear flow.

In figure 5a for $\delta < 0.15$ and in figure 5b for $-0.186 < \delta < -0.05$, the bifurcations are stationary with a large wave number which increases when δ decreases. The bifurcating structures are localized at the outer part of the cylinder as figures 5a and 5b display. In this range we can observe how for $\beta = 0.5$ the critical R_c decreases with δ while for $\beta = 5$ R_c tends to grow to infinity at the limit $\delta = -0.186$. This suggests that there is an asymptote where the critical R_c tends to infinity. This behavior corresponds to region III in the $\beta - \delta$ plane displayed in figure 6. Figure 3c) displays an example of a basic state in region III.

Finally for $\delta < -0.186$ and $\beta = 5$ no instability has been found in zone IV. This means that in this case there exist external parameter sets at which the axisymmetric basic state is very robust and does not bifurcate to 3D structures. This regime is surrounded by curve C_3 (dashed line) in the $\beta - \delta$ diagram in figure 6. Figure 3d) displays an example of a basic state in zone IV.

4.2.2 Influence of the rest of the parameters

Aspect ratio Γ . Results in previous subsections are based on a rather large aspect ratio domain ($\Gamma = 10$). At smaller aspect ratios the geometry of the domain has more influence on instabilities. Typically for uniform heating at smaller aspect ratios instability thresholds are larger than those obtained for larger aspect ratios and critical wave numbers are smaller. Figure 9 shows how the instability thresholds and wave numbers change with Γ . It is observed that the standard rules just described for the case of uniform heating are maintained,

although now oscillatory instabilities are possible. The same type of instabilities as those previously described are observed. We notice that in figure 9 for $\Gamma = 3$ a one-armed spiral is the most unstable mode while giant one-armed spirals described before, were found to be less preferred than target patterns with $k = 0$.

Pr number. Similar behaviors to those we have just described are also present for large and infinite Pr number. For instance the giant one-armed oscillatory spiral appears as well in a similar range of values of the parameters β and δ (see figure 8c) and with the same conditions, the mode $k = 1$ oscillatory is just below the instability threshold but very close to it, at the same parameter values.

4.3 Discussion and conclusions

We have studied how stationary and axisymmetric basic states bifurcate to different 3D structures depending on the shape factor β and temperature ratio $\delta = \Delta T_h / \Delta T_v$ appearing on the temperature boundary condition. The influence of horizontal and vertical temperature differences on instabilities has been addressed in numerous works [10, 14, 15, 16, 18, 20, 21, 22]; in our results a new heat parameter is introduced related to the shape of the applied heat. We have found that at each β , different δ values define zones with qualitatively different instabilities. Typically at small δ the basic state bifurcates to target and giant spiral wave patterns. The appearance of these structures is quite similar to those reported in experiments such as [2, 3, 4, 5] for the uniform heating case. The reason for this similitude might be the presence of a mean flow in those experiments close to our basic state, that could be caused by a non strictly uniform heat source. We find that even for infinite Prandtl number spiral patterns are present. Larger negative δ values originates very localized states at the outer part of the domain. Localized structures in the centre of the cell are found at small β values and positive δ values. A decreasing aspect ratio increases the instability threshold and decreases the critical wavenumber. This is in agreement with the uniform case which corresponds to $\delta = 0$.

Acknowledgements

This work was partially supported by the Research Grants MCYT (Spanish Government) BFM2003-02832, CCYT (JC de Castilla-La Mancha) PAC-05-005-01/02, MEC (Spanish Government), MTM2004-00797, SIMUMAT S-0505-ESP-0158 (Comunidad de Madrid) and by the University of Castilla-La Mancha. AMM acknowledges MCYT (Spanish Government) for a Ramón y Cajal Research Fellowship.

References

- [1] H. Bénard, “Les tourbillons cellulaires dans une nappe liquide.” *Rev. Gén. Sci. Pures Appl.* **11**, 1261 (1900).

- [2] E. Bodenschatz, J. R. de Bruyn, G. Ahlers, and D. S. Cannell, “Transitions between patterns in thermal convection”. *Phys. Rev. Lett* **67** 3078, (1991).
- [3] S.W Morris, E. Bodenschatz, D. S. Cannell and G. Ahlers, “Spiral defect chaos in large Aspect Ratio Rayleigh-Bénard convection”. *Phys. Rev. Lett* **71** 2026, (1993).
- [4] B. B. Plapp, D. A Egolf, E. Bodenschatz, W. Pesch, “Dynamics and selection of giant spirals in Rayleigh-Benard convection”. *Phys. Rev. Lett* **81** 5334 (1998).
- [5] M. Assenheimer, V. Steinberg, “Transition between spiral and target states in Rayleigh-Bénard Convection”. *Nature* **367** (6461) 345 (1994).
- [6] M. Bestehorn, M. Fantz, R. Friedrich, H. Haken, C. Perez-Garcia, “Spiral patterns in thermal convection”. *Zeitschrift fur Physik B-Condensed Matter* **88** (1): 93 (1992).
- [7] Xiao-jun Li, Hao-wen Xi, J.D. Gunton, “Dynamical properties of multiarmed global spirals in Rayleigh-Bénard convection”, *Phys. Rev. E* **54** R3105, (1996).
- [8] W. Pesch, “Complex spatiotemporal convection patterns” *Chaos* **6**, 348 (1996).
- [9] W. Decker, W. Pesch, and A. Weber “Spiral defect chaos in Rayleigh-Bnard convection” *Phys. Rev. Lett* **73** 648, (1994).
- [10] M. K. Smith and S. H. Davis, “Instabilities of dynamic thermocapillary layers. 1. Convective instabilities.” *J. Fluid Mech.* **132**, 119 (1983).
- [11] A. M. Mancho, H. Herrero and J. Burguete, “Primary instabilities in convective cells due to non-uniform heating.” *Phys. Rev E* **56**, 2916 (1997).
- [12] H. Herrero and A. M. Mancho “Influence of aspect ratio in convection due to non-uniform heating.” *Phys. Rev E* **57**, 7336 (1998).
- [13] R.J. Riley and G.P. Neitzel, “Instability of thermocapillary-buoyancy convection in shallow layers. Part 1. Characterization os steady and oscillatory instabilities.” *J. Fluid Mech* **359** , 143 (1998).
- [14] F. Daviaud and J.M. Vince, “Traveling waves in a fluid layer subjected to a horizontal temperature gradient.” *Phys. Rev. E* **48**, 4432 (1993).
- [15] J. Burguete, N. Mokolobwicz, F. Daviaud, N. Garnier and A. Chiffaudel, “Buoyant-thermocapillary instabilities in extended layers subjected to a horizontal temperature gradient.” *Phys. Fluids* **13**, 2773 (2001).
- [16] J. F. Mercier and C. Normand, “Buoyant-thermocapillary instabilities of differentially heated liquid layers.” *Phys. Fluids* **8**, 1433 (1996).

- [17] M.A. Pelacho and J. Burguete, “Temperature oscillations of hydrothermal waves in thermocapillary-buoyancy convection.” *Phys. Rev. E* **59**, 835 (1999).
- [18] A.M. Mancho and H. Herrero, “Instabilities in a lateraly heated liquid layer.” *Phys. Fluids* **12**, 1044 (2000).
- [19] A.B. Ezersky, A. Garcimartín, J. Burguete, H.L. Mancini and C. Pérez-García, “Hydrothermal waves in Marangoni convection in a cylindrical container.” *Phys. Rev. E* **47**, 1126 (1993).
- [20] S. Hoyas, H. Herrero and A.M. Mancho, “Thermal convection in a cylindrical annulus heated laterally.” *J. Phys. A: Math and Gen.* **35**, 4067 (2002).
- [21] S. Hoyas, H. Herrero and A.M. Mancho, “Bifurcation diversity of dynamic thermocapillary liquid layers.” *Phys. Rev. E*, **66**, 057301 (2002).
- [22] S. Hoyas, A.M. Mancho, H. Herrero, N. Garnier, A. Chiffaudel. “Bénard-Marangoni convection in a differentially heated cylindrical cavity” *Phys. Fluids*, **17**, 054104 (2005).
- [23] N. Garnier and A. Chiffaudel. “Two dimensional hydrothermal waves in an extended cylindrical vessel.” *Eur. Phys. J. B* **19**, 87 (2001).
- [24] N. Garnier and C. Normand. “Effects of curvature on hydrothermal waves instability of radial thermocapillary flows.” *C. R. Acad. Sci., Ser. IV* **2** (8) 1227 (2001).
- [25] E. Favre, L. Blumenfeld and F. Daviaud, “Instabilities of a liquid layer locally heated on its free surface.” *Phys. Fluids* **9**, 1473 (1997).
- [26] B.-C. Sim, A. Zebib. “Effect of free surface heat loss and rotation on transition to oscillatory thermocapillary convection.” *Phys. Fluids* **14** (1), 225 (2002).
- [27] B.-C. Sim, A. Zebib, D. Schwabe. “Oscillatory thermocapillary convection in open cylindrical annuli. Part 2. Simulations.” *J. Fluid Mech.* **491**, 259 (2003).
- [28] C. Bernardi and Y. Maday. Approximations spectrales de problèmes aux limites elliptiques. Springer-Verlag, Berlin, (1991).
- [29] C.Canuto, MY Hussaine, A. Quarteroni, TA Zang. Spectral Methods in Fluid Dynamics. Springer: Berlin, 1988.
- [30] H. Herrero and A.M. Mancho, “On pressure boundary conditions for thermoconvective problems.” *Int. J. Numer. Meth. Fluids* **39**, 391 (2002).
- [31] S. Hoyas. Estudio teórico y numérico de un problema de convección. Thesis, Universidad Complutense de Madrid, 2003.

- [32] N. Garnier. Ondes non-linéaires à une et deux dimensions dans une mince couche de fluide. Thesis, University Paris 7 Denis Diderot, 2000.
- [33] M.C. Navarro, A. Wathen, A. M. Mancho, H. Herrero. *Journal of Computational Physics* submitted.

Figure captions

Figure 1

Physical set-up.

Figure 2

Temperature boundary conditions at the bottom for $\Gamma = 10$; a) for $\delta = 1$ and different values of β ; b) for $\beta = 0.5$ and different values of δ .

Figure 3

a) Isotherms and velocity field of the basic state corresponding to values of the parameters $R = 356880$, $\Gamma = 10$, $Pr = 0.4$, $B = 0.05$, $\delta = 0.25$ and $\beta = 0.5$; b) isotherms and velocity field of the basic state corresponding to values of the parameters $R = 19064$, $\Gamma = 10$, $Pr = 0.4$, $B = 0.05$, $\delta = 0.05$ and $\beta = 5$; c) isotherms and velocity field of the basic state corresponding to values of the parameters $R = 30377$, $\Gamma = 10$, $Pr = 0.4$, $B = 0.05$, $\delta = 0.15$ and $\beta = 0.5$; d) isotherms and velocity field of the basic state corresponding to values of the parameters $R = 10250$, $\Gamma = 10$, $Pr = 0.4$, $B = 0.05$, $\delta = -0.6$ and $\beta = 5$.

Figure 4

Maximum real part of the growth rate λ as a function of k for basic state at threshold $R_c = 15095$, the rest of the parameters are $\Gamma = 10$, $Pr = 0.4$, $B = 0.05$, $\delta = 0.05$ and $\beta = 0.5$. The maximum determines the critical $k_c = 15$. Void circles correspond to real eigenvalues while crossed ones stand for complex eigenvalues.

Figure 5

a) Critical R , wave number k values and growing modes as a function of δ for $\beta = 0.5$. Remaining external parameters are $\Gamma = 10$, $Pr = 0.4$ and $B = 0.05$; b) the same for $\beta = 5$. Void circles correspond to stationary instabilities while crossed ones stand for oscillatory instabilities; c) A zoom of zones II and III of b). Dashed vertical lines correspond to the asymptotes.

Figure 6

Different regions of bifurcations in the $\beta - \delta$ plane. The rest of the parameters are $\Gamma = 10$, $Pr = 0.4$ and $B = 0.05$.

Figure 7

Maximum real part of the growth rate λ as a function of k for basic state at threshold $R_c = 19064$ corresponding to the target ($k_c = 0$) and the giant one-armed spiral ($k = 1$) just below the instability threshold but very close to it. The rest of the parameters are $\Gamma = 10$, $Pr = 0.04$, $B = 0.05$, $\delta = 0.05$ and $\beta = 5$. Void circles correspond to real eigenvalues while crossed ones stand for complex eigenvalues.

Figure 8

a) Target at the instability threshold $R = 19064$. The rest of the parameters are $\Gamma = 10$, $Pr = 0.4$, $B = 0.05$, $\delta = 0.05$, and $\beta = 5$; b) giant one-armed spiral just below the instability threshold but very close to it, at the same parameter values; c) giant one-armed spiral for $Pr = \infty$, the rest of the parameters are $R = 4674$, $\Gamma = 10$, $B = 0.2$, $\delta = 0.1$ and $\beta = 5$.

Figure 9

Critical R , wave number k values and growing modes as a function of Γ for $\beta = 0.5$, $Pr = 0.4$, $B = 0.05$ and $\delta = 1$.

Table captions

Table I

Critical Rayleigh numbers R_c for different orders of expansions in Chebyshev polynomials. The critical wave number is $k_c = 0$ and the parameters are $\Gamma = 10$, $Pr = 0.4$, $\delta = 0.05$, $B = 0.05$ and $\beta = 5$.

	$N = 9$	$N = 11$	$N = 13$	$N = 15$	$N = 17$
$L = 19$	19069	19070	19070	19070	19070
$L = 25$	19055	19056	19056	19056	19056
$L = 29$	19065	19066	19066	19066	19066
$L = 33$	19063	19064	19064	19064	19064
$L = 37$	19063	19064	19064	19064	19064

Figure 1

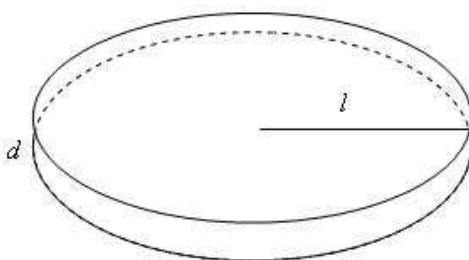


Figure 2

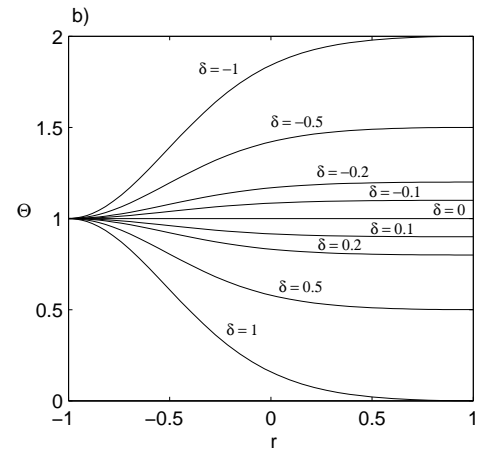
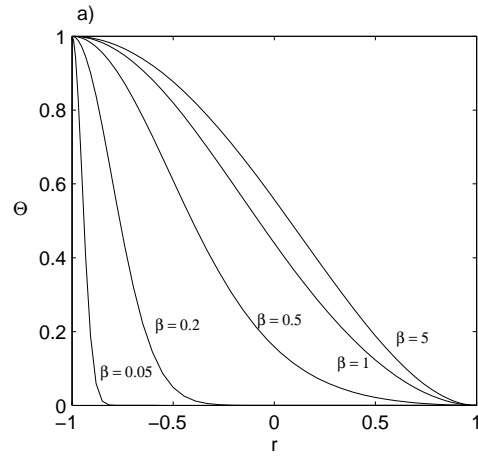


Figure 3

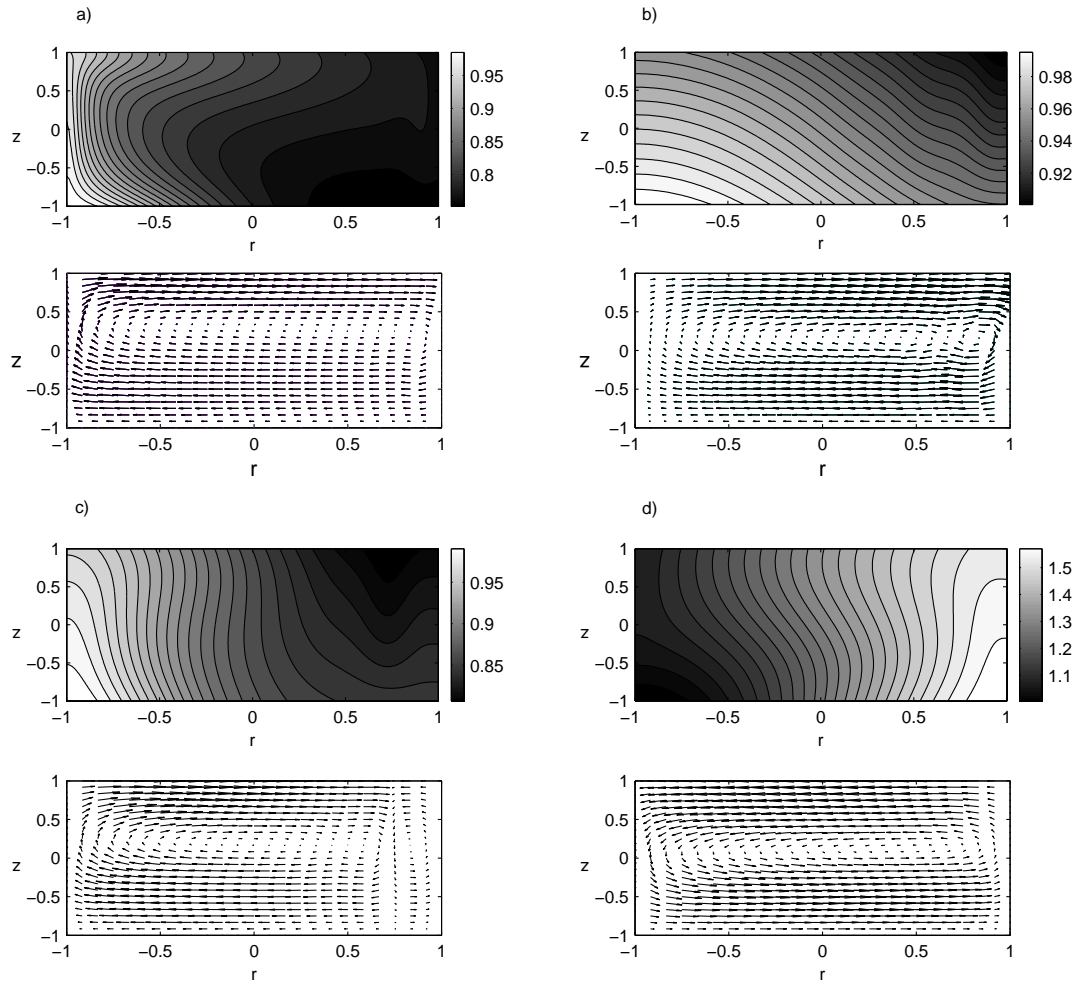


Figure 4

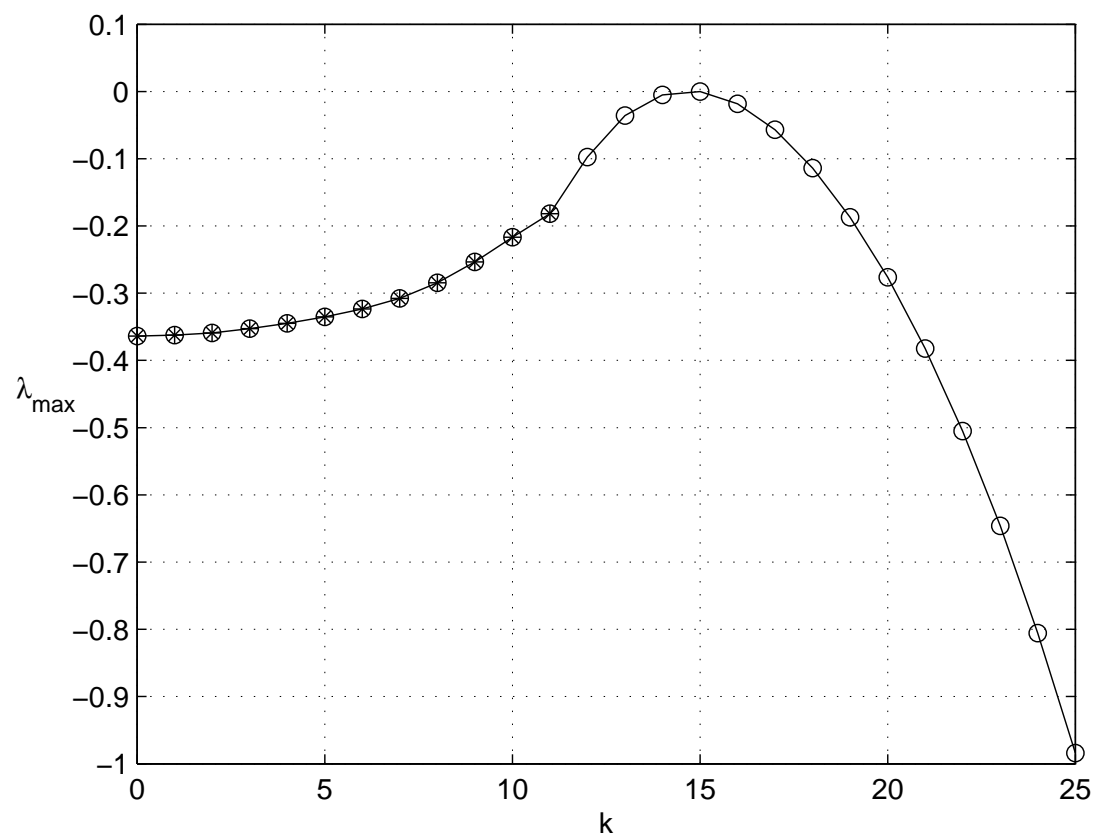


Figure 5

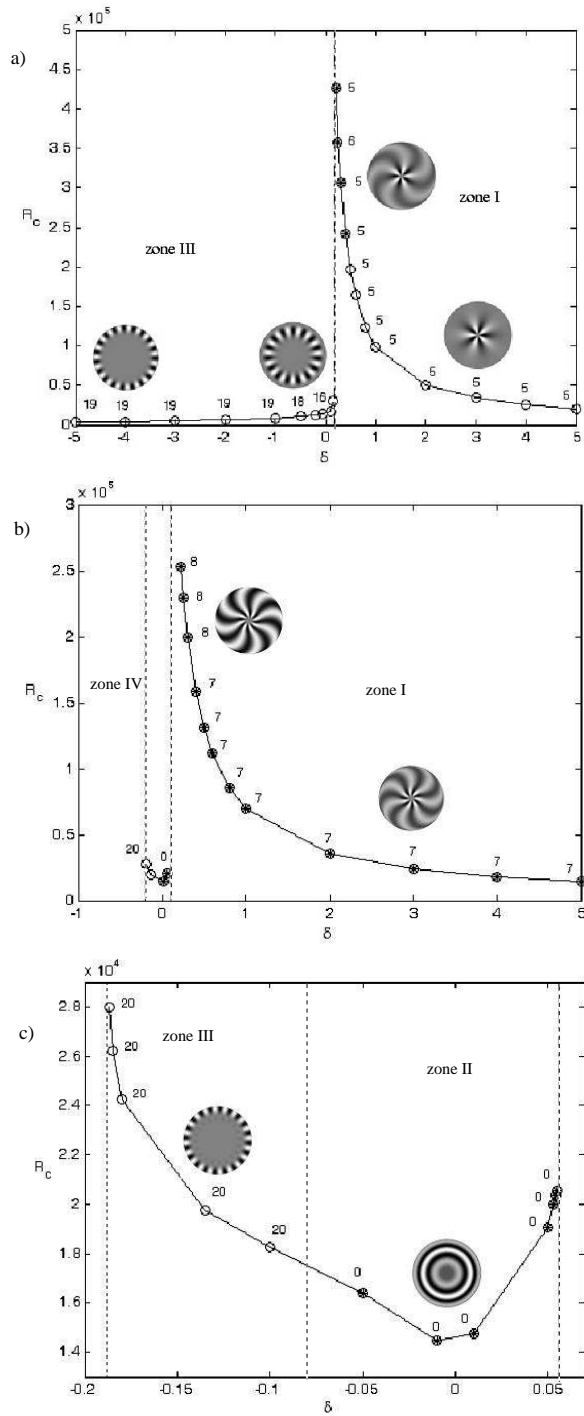


Figure 6

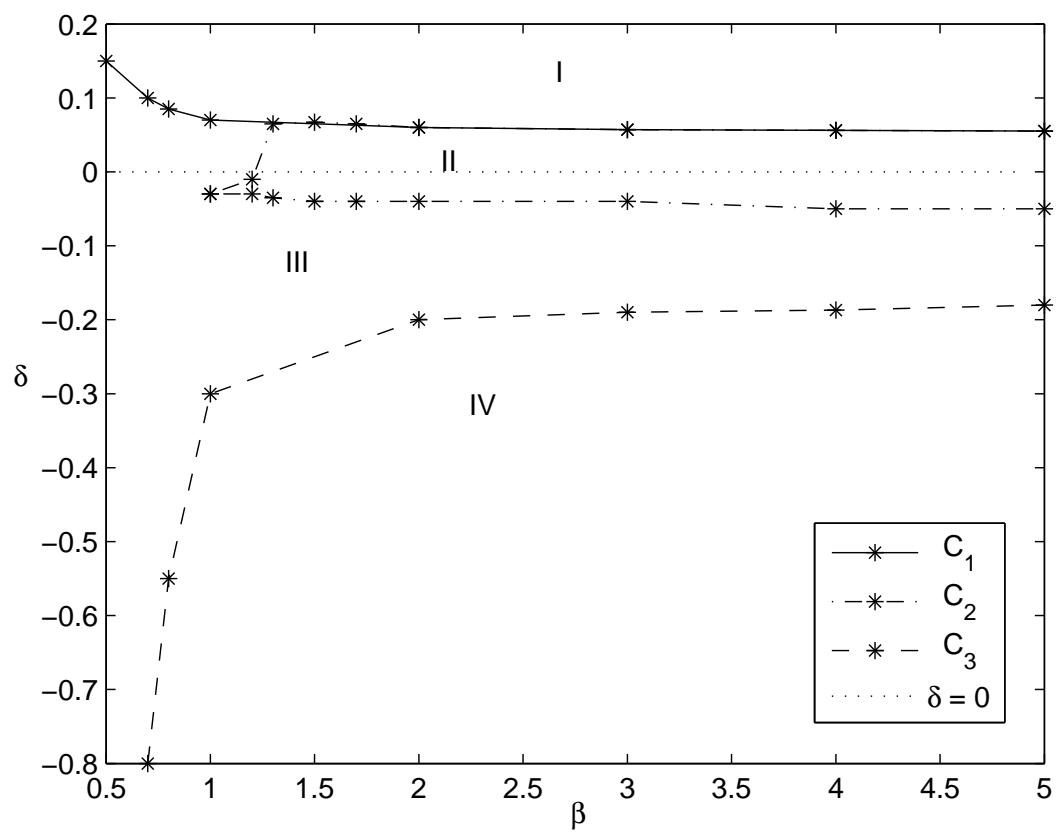


Figure 7

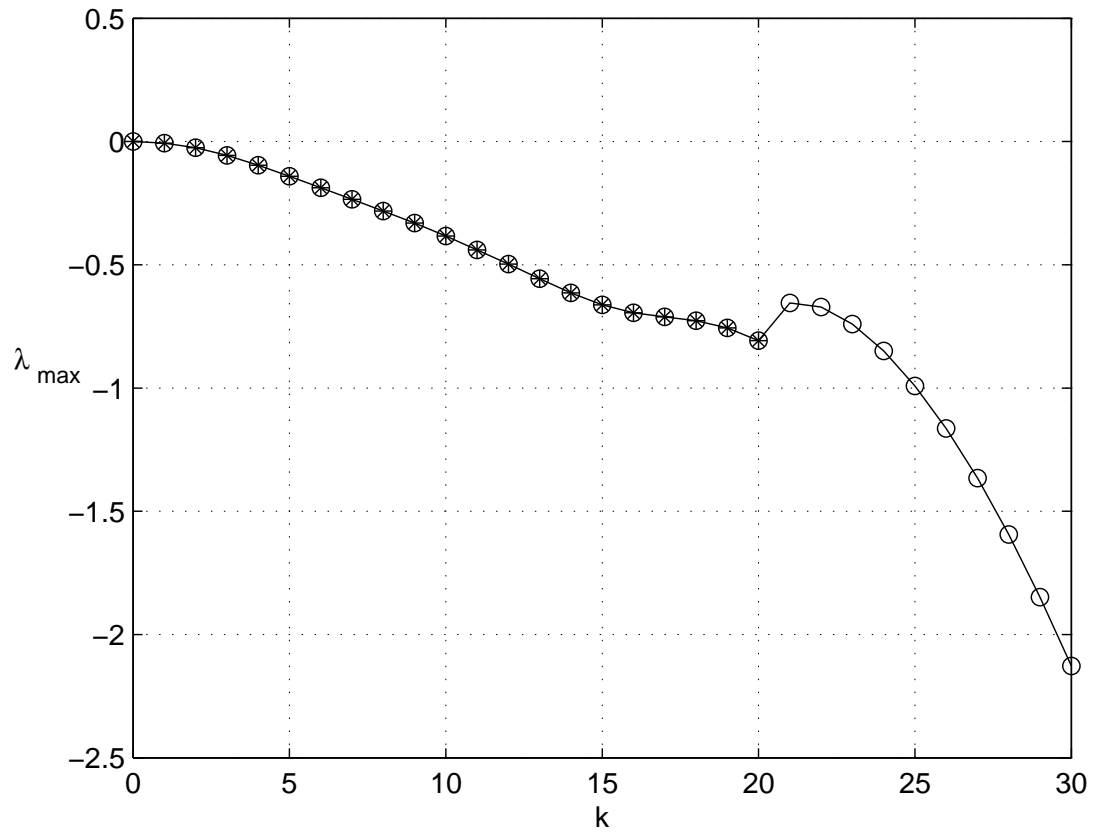


Figure 8

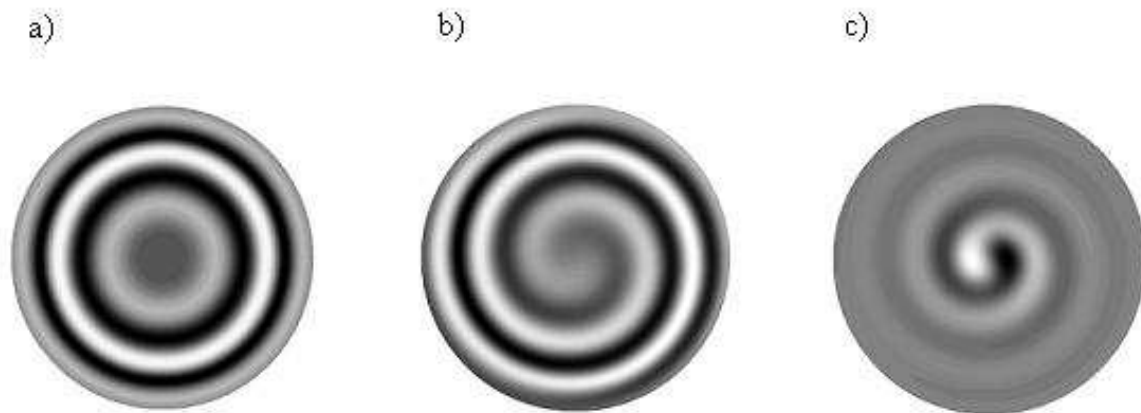


Figure 9

